Dalton Transactions

ROYAL SOCIETY OF CHEMISTRY

PAPER

View Article Online
View Journal | View Issue

Cite this: *Dalton Trans.*, 2026, **55**, 5511

Chalcogen bond activation in cation radical salts of naphthalene *peri*-diselenides with *S* = 5/2 magnetic anions

Hrudya Pariyacheri Padikkal,[a] Olivier Jeannin, [a] Mathieu Rouzières,[b] Rodolphe Clérac, [b] Ie-Rang Jeon *[b] and Marc Fourmigué *[a]

Received 2nd February 2026,
Accepted 5th March 2026

DOI: 10.1039/d6dt00277c

rsc.li/dalton

The activation of strong σ-holes in the oxidized form of 2,7-dimethoxynaphthalene *peri*-diselenide (**1**) is demonstrated in its radical salts with magnetic (*S* = 5/2) FeX_4^- anions as well as their diamagnetic analogs GaX_4^- (X = Cl, Br). All four salts exhibit short and directional Se···X chalcogen bonding (ChB) interactions, together with strong dimerization of the radical species into dicationic dimers along the stacks of $\mathbf{1}^{\bullet+}$. Magnetic analysis highlights the presence of antiferromagnetic interactions between paramagnetic FeX_4^- anions and reveals long-range antiferromagnetic order with T_N = 5.9 K only in the $FeBr_4^-$ salt, attributable to the short Br···Br distances induced by ChB interactions.

Introduction

The solid-state chemistry of π-type radicals[1] is based on a combination of (i) intermolecular interactions found in any molecular solid (van der Waals interactions, π–π interactions, hydrogen/halogen/chalcogen bonding)[2] and (ii) overlap interactions of the SOMO of such open-shell species. The outcome of such combined interactions governs their magnetic properties, encompassing non- or weakly interacting species, strongly dimerized systems, and extended systems exhibiting long-range magnetic correlations.[3] Among π-type radicals, cationic species such as those derived from tetrathiafulvalene (TTF) derivatives occupy a special place in this landscape, as (i) they can crystallize into mixed-valence, highly conducting salts,[4] and (ii) oxidation to the radical cation state activates the TTF substituents, enabling enhanced supramolecular interactions through stronger hydrogen, halogen or chalcogen bonding. This has been revealed recently through substitution of the TTF core with halogens (I, Br),[5,6] or selenomethyl (SeMe) moieties,[7] as the oxidation of the TTF strongly reinforces the σ-hole in the prolongation of the C_{TTF}–I or C_{TTF}–Se bond, for interactions with the counter ion (Cl^-, Br^-, ClO_4^-, $TCNQF_n^-$, ...) acting as Lewis base. One added value to these directional interactions could be the association of such activated TTFs cation radicals (*S* = 1/2) with paramagnetic anions such as the prototypical *S* = 5/2 $Fe^{III}Cl_4^-$. Such systems are indeed expected to favor so-called π–d interactions between the delocalized π-type conducting electrons of the donor and the localized d-type magnetic anions.[8,9] The emergence of delicately balanced such π–d interactions can indeed give rise to intriguing spin-charge coupled phenomena, such as giant magnetoresistance and field-induced superconductivity.[10] Along this line, the introduction of halogen bonding have also proven successful in controlling intermolecular interactions between donor and FeX_4^- anions, as illustrated in $(EDO\text{-}TTFBr_2)_2FeX_4$ (X = Cl, Br) salts and analogs.[11,12] However, this attractive approach is hampered by the spin density distribution in iodo- and selenomethyl-substituted TTFs, essentially localized on the central C_2S_4 TTF moiety, with very small spin density on outer halogen/chalcogen substituents.[7] As a consequence, direct magnetic interactions are very limited. In order to circumvent this issue, we turn our interest to non-TTF-based electron donors where both HOMO and spin density distribution will be concentrated on those atoms prone to simultaneously act as halogen- or chalcogen bond donors. We accordingly considered electron-rich diselenides and tetraselenides such as **1–4**.

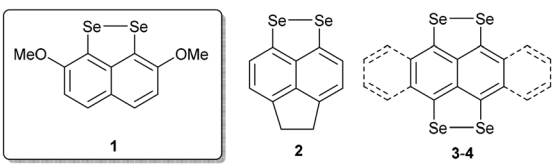

Indeed, as shown in Fig. 1 for compound **1** (2,7-dimethoxynaphthalene *peri*-diselenide), the HOMO and spin density are highly concentrated on the selenium atoms. Furthermore, cal-

[a]*Univ. Rennes, CNRS, ISCR (Institut des Sciences Chimiques de Rennes), UMR 6226 F-35042 Rennes, France. E-mail: marc.fourmigue@univ-rennes.fr*
[b]*Univ. Bordeaux, CNRS, CRPP, UMR 5031 F-33600 Pessac, France. E-mail: ie-rang.jeon@u-bordeaux.fr*

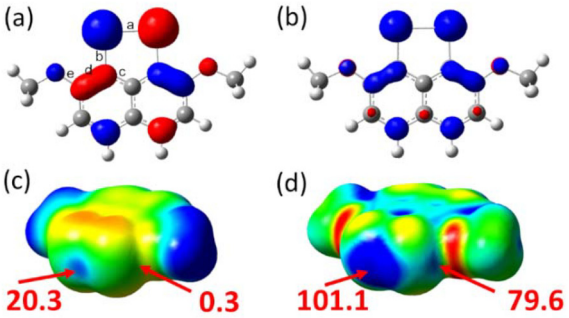

Fig. 1 Electronic properties of **1** with (a) HOMO, (b) spin density distribution in $\mathbf{1}^{\bullet+}$, ESP surface of (c) neutral **1**, and (d) ESP surface of radical cation ($\mathbf{1}^{\bullet+}$) with $V_{s,max}$ values reported in kcal mol^{-1}.

culated electrostatic potential (ESP) surface of the cation radical $\mathbf{1}^{\bullet+}$ shows the presence of σ-holes located in the molecular plane and able to interact with anions through ChB, two in the prolongation of the Se–Se bond, and one perpendicular to this Se–Se bond, corresponding to the merging of the two individual σ-holes in the prolongation of the C–Se bonds. We have already shown that such σ-hole localization is general among cyclic diselenides,[13,14] and we demonstrate here that their amplitude is strongly enhanced when going from the neutral (Fig. 1c) to the cation radical state (Fig. 1d). Also, we noticed that compounds **3** and **4** in their reported chloride salts,[15,16] are indeed engaged in short Se···Cl$^-$ ChB.

In that respect, the diselenide **1** was reported to form only *neutral* charge transfer complexes with TCNQ, without any report on their crystal structures.[17] We demonstrate here that **1** can be successfully oxidized into stable cation radicals, which were isolated in the present work with magnetic (S = 5/2) FeX_4^- anions as well as their diamagnetic analogs GaX_4^- (X = Cl, Br), affording the corresponding 1 : 1 salts, characterized with strong antiferromagnetic interactions and a long-range antiferromagnetically ordered ground state for the $FeBr_4^-$ salt.

Results and discussion

Donor molecule **1** was prepared as previously described[18] from 1,8-dibromo-2,7-dimethoxynaphthalene, with minor modifications reported in SI. Its oxidation potential was measured at 0.62 V *vs.* SCE in CH_2Cl_2 (+0.18 V *vs.* Fc^+/Fc).[17a] Electrocrystallization experiments were conducted with the *n*-Bu_4N^+ salts of $FeCl_4^-$ and $FeBr_4^-$, and their diamagnetic analogs $GaCl_4^-$ and $GaBr_4^-$, affording four salts with 1 : 1 stoichiometry, formulated as (**1**)(FeX_4) or (**1**)(GaX_4). As shown in Table S1, the salts with $FeCl_4^-$, $FeBr_4^-$ and $GaBr_4^-$ are isostructural. They crystallize in the monoclinic system, space group $P2_1/n$ with both $\mathbf{1}^{\bullet+}$ cation and anion in general position. The $GaCl_4^-$ crystallizes in the triclinic system, space group $P\bar{1}$, with both $\mathbf{1}^{\bullet+}$ cation and anion in general position but with the $GaCl_4^-$ anion disordered on two positions with a 91 : 9 distribution. The overall solid-state organization of the cation and the anion in (**1**)($GaCl_4$) is however closely related to that of the three other salts (*vide infra*). Note that a second phase of (**1**)($GaCl_4$), denoted (**1**)($GaCl_4$)_B was identified concomitantly. It crystallizes in the triclinic group $P\bar{1}$, with twice the volume of the former one, two independent $\mathbf{1}^{\bullet+}$ cations and two independent, disordered $GaCl_4^-$ anions. It is described in more details in SI (Fig. S3–S6).

We note sizeable evolutions of the intramolecular bond distances in $\mathbf{1}^{\bullet+}$, when compared with its neutral counterpart **1** (Table S4). It appears indeed that the bonds a (Se–Se), b (C–Se) and e (C–OMe), of antibonding nature in the HOMO of **1** (*cf.* Fig. 1a in which the bond notation is also given) shorten upon oxidation (−1.4, −1.7 and −2.3% respectively), while bonds d (C–C), of bonding nature in the HOMO, lengthen upon oxidation by +2.4%. The bonds c (C–C) are not modified, consistent with their nonbonding nature in the HOMO as one C atom is located on an orbital node.

A view of the unit cell of (**1**)($FeCl_4$) is shown in Fig. 2 as a representative example of the four salts (see Fig. S7–S9). The salts are characterized by stacks of cation radicals running along the *a* direction. Along the stacks, the molecules adopt two different inversion-centered head-to-tail overlaps (Fig. 2b and c), with very different interplanar distances, found in (**1**)($FeCl_4$) at 3.19 and 3.49 Å, in (**1**)($GaCl_4$) at 3.21 and 3.47 Å, in (**1**)($FeBr_4$) at 3.20 and 3.51 Å, and in (**1**)($GaBr_4$) at 3.21 and 3.51 Å. The intra-dimer plane-to-plane distances (3.19–3.21 Å) are notably shorter than the C···Se van der Waals contact distances (3.60 Å), indicating a strong dimerization of the S = 1/2 radical species into dicationic dimers in all salts.

The dimerized chains are surrounded by the Fe/GaX_4^- anions, with short and directional Se···X (X = Cl, Br) contacts characteristic of ChB interactions. Indeed, as detailed in Fig. 3 for (**1**)($FeCl_4$), two Cl atoms (Cl1 and Cl4) lie in the molecular

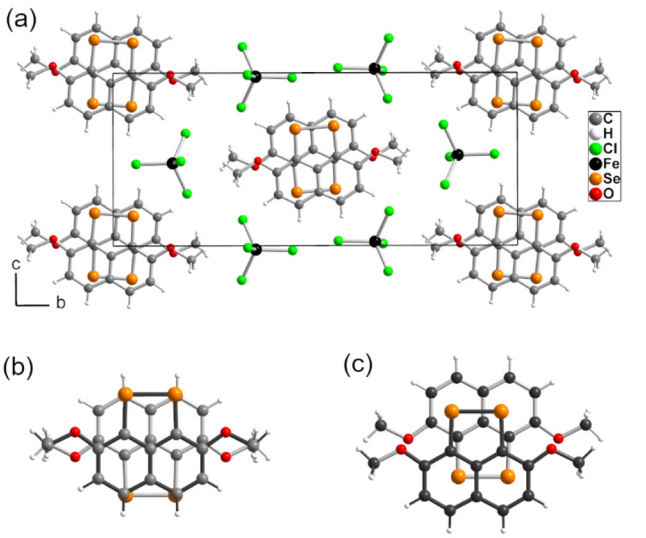

Fig. 2 Structure of (**1**)($FeCl_4$) with: (a) projection view of the unit cell along *a*, (b) intra-dimer overlap pattern with a plane-to-plane distance of 3.19 Å, and (c) inter-dimer overlap pattern with a plane-to-plane distance of 3.49 Å.

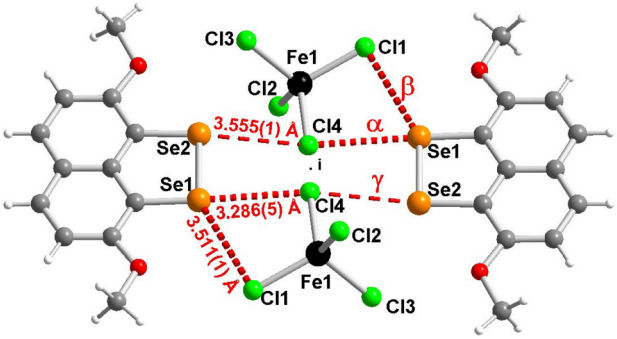

Fig. 3 Detail of the ChB interactions (red dotted lines) in (**1**)($FeCl_4$).

plane of the donor molecule, allowing for the setting of two ChB interactions with Se1, noted α and β in Fig. 3, at 3.286(5) and 3.511(1) Å, corresponding to a reduction ratio (RR) of respectively 0.90 and 0.96. A third ChB interaction (noted γ) with the inversion-related $FeCl_4^-$ anion is observed between Se2 and Cl4 (RR = 0.97). This organization pattern is essentially similar in the other salts (see Fig. S10–S12 in SI), with variations associated with the smaller size of $GaCl_4^-$, with the larger radius of Br in the $FeBr_4^-$ and $GaBr_4^-$ anions. ChB distances are collected in Table 1.

Transport measurements performed on single crystals by the two-point method show for all four salts an essentially insulating behavior with σ_{RT} values of 8.1×10^{-7} and 1.9×10^{-8} S cm^{-1} in the $FeCl_4^-$ and $FeBr_4^-$ salts respectively, and 2.3×10^{-8} and 8.0×10^{-9} S cm^{-1} in the $GaCl_4^-$ and $GaBr_4^-$ salts respectively. These values confirm the very strong dimerization of the $\mathbf{1}^{\bullet+}$ radicals within the stacks.

Magnetic susceptibility (χ) measurements performed on a polycrystalline sample of the two $GaCl_4^-$ and $GaBr_4^-$ salts indicate their diamagnetic behavior. This confirms the analysis made above based on the crystal structures and shows that the S = 1/2 $\mathbf{1}^{\bullet+}$ radicals are strongly paired into the dimerized chains and do not contribute to the magnetism below 300 K. This result implies that the magnetic response of the two $FeCl_4^-$ and $FeBr_4^-$ salts is attributable only to the contributions of the inorganic anions.

To probe and compare magnetic behaviors of the two $FeCl_4^-$ and $FeBr_4^-$ salts, variable-temperature dc magnetic susceptibility data were collected for microcrystalline samples. The resulting plot of χT *vs.* T is shown in Fig. 4. At 300 K, the χT value is 4.4 cm^3 K mol^{-1} for both compounds, in good agreement with the expected contribution of a high-spin S = 5/2 Fe^{III} ion (C = 4.375 cm^3 K mol^{-1} with g = 2; g being the

Table 1 Se···X (X = Cl, Br) ChB distances in the four salts

	α ChB (Å), RR	β ChB (Å), RR	γ ChB (Å), RR
(**1**)($FeCl_4$)	3.286(5), 0.90	3.511(1), 0.96	3.555(1), 0.97
(**1**)($GaCl_4$)	3.255(11), 0.89	3.503(6), 0.96	3.593(7), 0.98
(**1**)($FeBr_4$)	3.377(5), 0.90	3.634(1), 0.97	3.750(1), 1.00
(**1**)($GaBr_4$)	3.413(9), 0.91	3.658(2), 0.97	3.734(1), 0.99

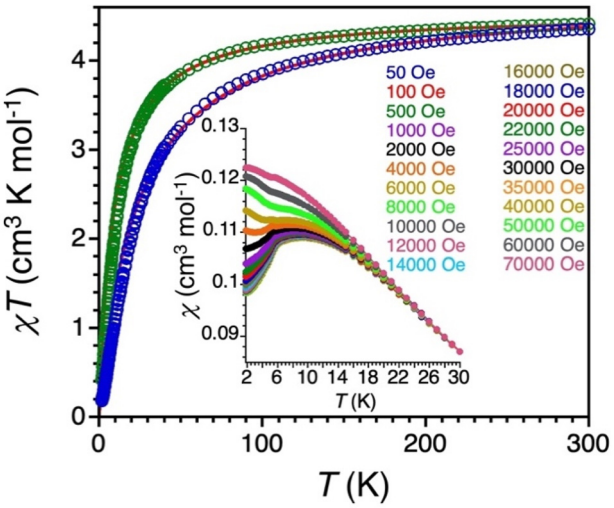

Fig. 4 Temperature dependence of the χT product measured at 0.1 T for the $FeCl_4^-$ (in green open circles) and $FeBr_4^-$ (in blue open circles) salts (where $\chi = M/H$ is the magnetic susceptibility normalized per mole of formula unit, *i.e.* per one mole of Fe center). The solid red lines are the best fits of the experimental data between 25 and 300 K to the Curie–Weiss law, leading to C = 4.54 and 4.71 cm^3 K mol^{-1} and θ = −9.1 and −23.2 K, for the $FeCl_4^-$ and $FeBr_4^-$ salts, respectively. Inset: temperature dependence of the molar magnetic susceptibility for a polycrystalline sample of the $FeBr_4^-$ salt at different dc fields up to 7 T. Solid lines are guides for the eye.

Landé factor). Upon lowering temperature, the χT product gradually decreases, reaching values of 0.4 and 0.2 cm^3 K mol^{-1} at 1.85 K for the $FeCl_4^-$ and $FeBr_4^-$ salts, respectively. Such thermal behavior indicates the presence of predominant antiferromagnetic interactions between the Fe^{III} spins. Notably, the χT product of the $FeBr_4^-$ salt falls at higher temperature than that of the $FeCl_4^-$ salt, suggesting stronger antiferromagnetic interactions in the former.

Indeed, the plot of χ^{-1} *vs.* T (Fig. S13 in SI) displays a linear relationship in the 30–300 K temperature range, consistent with a Curie–Weiss law (g = 2.0 and 2.1 and θ = −9.1 and −23 K for the $FeCl_4^-$ and $FeBr_4^-$ salts, respectively), thereby confirming the stronger antiferromagnetic interaction in the $FeBr_4^-$ salt.

To further investigate the low temperature magnetic behavior, variable-field magnetization data were collected for both compounds below 15 K as shown in Fig. 5. At 1.85 K, the M *vs.* H data are non-linear for both compounds, reaching 3.8 and 1.6 μ_B at 7 T for the $FeCl_4^-$ and $FeBr_4^-$ salts, respectively. These values are significantly lower than the expected saturation value of 5 μ_B, particularly in the case of the $FeBr_4^-$ salt. The deviation from linear field dependence is highlighted by a broad maximum in the dM/dH *vs.* H plot for the $FeCl_4^-$ salt (Fig. S14). This feature is nearly independent of temperature and does not extrapolate to zero at finite temperature, likely indicating the presence of antiferromagnetic interactions between Fe^{III} centers that are compensated by the applied magnetic field at $H^*(0)$ = 4.25 T (value extrapolated at zero).

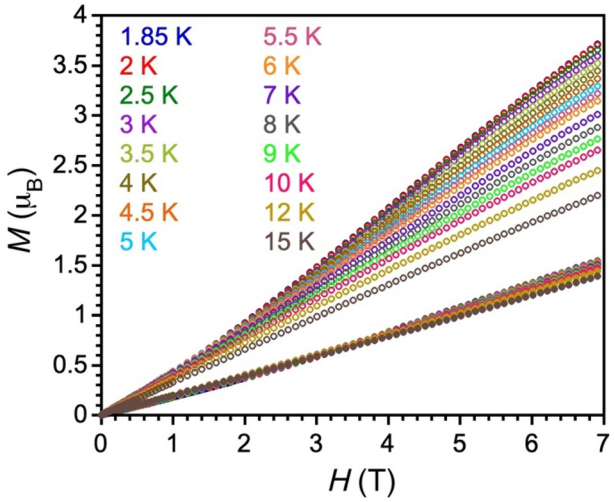

Fig. 5 Field dependence of the magnetization up to 7 T at indicated temperatures between 1.85 and 15 K for the $FeCl_4^-$ (in open circles) and $FeBr_4^-$ (in full circles) salts.

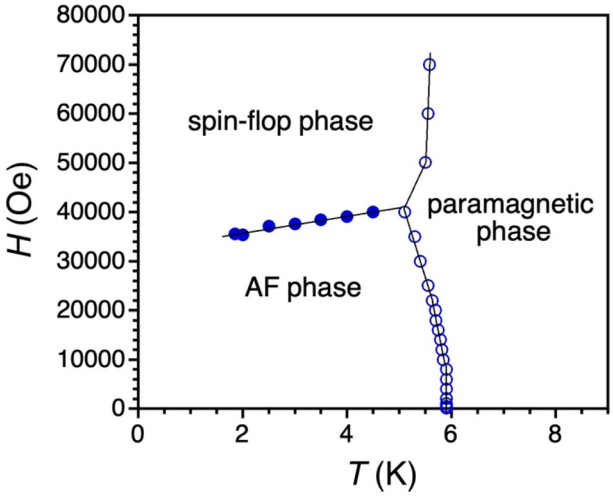

Fig. 6 (*T*, *H*) phase diagram for the $FeBr_4^-$ salt. Full circles: location of the maximum of susceptibility from d*M*/d*H* *vs.* *H* data (Fig. S15); open circles: location of the maximum of susceptibility from χ *vs.* *T* data (Fig. 4 inset). The solid lines are guides.

The average magnetic exchange is estimated at $zJ'/k_B = -1.1$ K from the field/interaction energy equality, $g\mu_B SH^*(0) = 2|zJ'|S^2$.[19] It is worth mentioning that, despite the observance of H^* and the field-dependence shown in χ *vs.* *T* data (Fig. S15; or non-linearity of the *M* *vs.* *H* data), an ordered antiferromagnetic ground state was not observed in the $FeCl_4^-$ salt above 1.85 K.

In contrast, the d*M*/d*H* *vs.* *H* plot of the $FeBr_4^-$ salt shows a sharp peak at 1.85 K (Fig. S16). Moreover, χ *vs.* *T* data reveal strong field-dependence with a pronounced low-temperature drop at low fields (Fig. 4 inset). By combining *M* *vs.* *H* and χ *vs.* *T* data, and taking the maximum of the d*M*/d*H* *vs.* *H* and χ *vs.* *T* plots, the characteristic field, H_C, was tracked to construct a (*T*, *H*) phase diagram, shown in Fig. 6. The extrapolation of the characteristic field to zero at a finite temperature confirms the presence of an 3D antiferromagnetic order with $T_N = 5.9$ K. When a magnetic field is applied, a transition line corresponding to H_{C1} emerges, that is only weakly temperature dependent. At higher magnetic fields, $H > H_{C1}$, a quasi-vertical transition line continues around 5.6 K. This observation, together with the gradual magnetization increase under applied dc field, suggests the presence of three different magnetic phases with an antiferromagnetic (AF)-to-spin-flop (SF) phase transition at H_{C1},[20] resulting from the competition between anisotropy (E_a) and the Zeeman energies.[21] H_{C2} corresponding to the SF-to-paramagnetic phase transition is not accessible in the experimental window of dc fields. Nevertheless, neglecting anisotropy contribution on H_{C2} ($H_E \gg H_A$, where H_A and H_E are anisotropy and exchange fields, respectively) this field can be estimated from the perpendicular susceptibility, χ_{perp}, obtained experimentally by the slope of the *M* *vs.* *H* data at 1.85 K at $H > H_{C1}$: $H_{C2} \approx Ng\mu_B S/\chi_{perp} \approx 21$ T.

A quantitative analysis of the effect of the applied field is possible at $T = 0$ K where entropy vanishes, and the expressions for $H_{C1}(0)$ and $H_{C2}(0)$ are given by the following equations for $g = 2$:[22]

$$H_{C1}(0)^2 = 2H_A H_E - {H_A}^2 \quad (1)$$

$$H_{C2}(0) = 2H_E - H_A \quad (2)$$

By taking $H_{C1}(0) = 3.36$ T, extrapolated from the phase diagram, and $H_{C2}(0) \approx 21$ T, H_A and H_E are estimated to 0.54 T and 10.8 T. From these molecular fields, an estimation of the magnetic anisotropy and the exchange interactions can be given: $|D|/k_B = 0.14$ K and $zJ'/k_B \approx -2.9$ K, justifying the weak anisotropy limit, $|zJ'| \gg |D|$ (with $g\mu_B SH_A = 2DS^2$ and $g\mu_B SH_E = 2|zJ'|S^2$). Note that the estimated magnetic exchange in the $FeBr_4^-$ salt is about twice as large as that estimated for the $FeCl_4^-$ salt, likely explaining the observation of the ordered magnetic ground state of the former.

These magnetic analyses are indeed consistent with the X···X contact distances observed in the structures of both compounds. The closest X···X interactions occur between inversion-related FeX_4^- anions at 3.409(1) and 3.482(1) Å for the $FeCl_4^-$ and $FeBr_4^-$ salts (Fig. 7 and Fig. S17), respectively. These distances correspond to RR values of 0.97 and 0.94, indicating stronger interactions between $FeBr_4^-$ anions. Moreover, the next closest Cl···Cl distances in the $FeCl_4^-$ salt amount to 4.122(5) Å along the crystallographic *a* direction and 4.425(3) Å in the *bc* plane. The equivalent Br···Br distances in the $FeBr_4^-$ salt are shorter, 4.058(5) and 4.254(3) Å, despite the larger radius of Br. Taken together, the shorter and more effective Br···Br contacts in three dimensions in the $FeBr_4^-$ salt explain the stabilization of an 3D antiferromagnetic order, whereas the relatively longer Cl···Cl contacts in the $FeCl_4^-$ salt limit the interactions to short-range correlations, thereby inhibiting the development of long-range magnetic order. The origin of such antiferromagnetic interactions has been attribu-

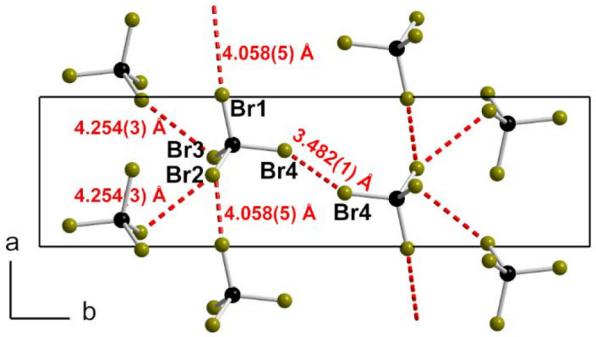

Fig. 7 Detail of the Br···Br interaction network in (**1**)($FeBr_4$).

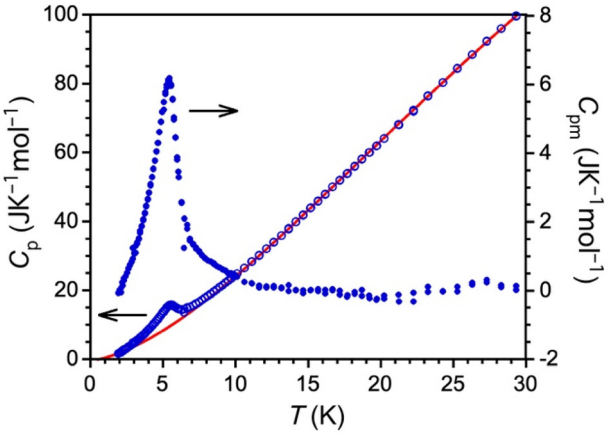

Fig. 8 Open circles: temperature dependence of the heat capacity, C_p, per mole of the $FeBr_4^-$ salt measured on a polycrystalline sample under zero applied field. The red solid line corresponds to the empirical polynomial base line used to determine the non-magnetic background of the heat capacity ($C_{p,background}$). Full circles: temperature dependence of the magnetic component (C_{pm}) of the heat capacity deduced from $C_{pm} = C_p - C_{p,background}$.

ted in some instances to so called π–d interactions, where the cation radicals would mediate indirect interactions between the S = 5/2 species.[23] However, the short Br···Br and Cl···Cl interactions found here lead us to rule out this possibility. On the other hand, a CCDC search for halogen–halogen intermolecular contacts between MX_4^- anions (M = Fe, Ga; X = Cl, Br) shows that the averaged X···X distances amount to 3.516 Å and 3.552 Å in $GaCl_4^-$ and $FeCl_4^-$ salts, to 3.602 Å and 3.629 Å in $GaBr_4^-$ and $FeBr_4^-$ respectively. The notably shorter distances found here in (**1**)($FeCl_4$) and particularly in (**1**)($FeBr_4$) [3.482(1) Å] demonstrate that the Se···X ChB interactions with the $\mathbf{1}^{\bullet+}$ cation radicals play an important role in bringing close to each other the S = 5/2 metalate anions. Such effects were discussed in isostructural salts of $FeCl_4^-$ and $FeBr_4^-$ with tetramethylammonium[24] or 2-methylquinolinium[25] counter ions. In such systems and despite larger Br···Br than Cl···Cl intermolecular distances, stronger antiferromagnetic interactions are also observed with $FeBr_4^-$. Also, in cation radical salts of tetrathiafulvalenes derivatives with $FeCl_4^-$ and $FeBr_4^-$,[26] the stronger antiferromagnetic interaction with the latter (and stabilization of an antiferromagnetic ground state) was indeed attributed to the increase of the "d–p mixing" between 3d orbitals of Fe and 4p orbitals of Br atoms and the large electron cloud of Br atom in the $FeBr_4^-$ salt,[27] which enhance the intermolecular magnetic interaction through halogen atoms compared to the $FeCl_4^-$ salt.

To cross-check the presence of the magnetic phase transition at low temperatures, heat capacity measurements were performed on both compounds between 2 and 50 K. As shown in Fig. 8, a reproducible λ-type feature is observed for the $FeBr_4^-$ salt, confirming the presence of an ordered magnetic ground state. In contrast, the appearance of a broad feature around 2 K in the $FeCl_4^-$ salt is likely due to the short-range order effect,[28] which is consistent with the magnetic data (Fig. S18). In order to further analyze these calorimetric measurements, the magnetic component of the heat capacity (C_{pm}) was extracted by subtracting the baseline, which should mainly correspond to the lattice contribution and was modeled to an empirical polynomial expression. While this correction was reasonably applied to the $FeBr_4^-$ salt (Fig. 8), the broad low temperature rise of C_p in the $FeCl_4^-$ salt made the fit inherently less precise, which in turn could lead to significant errors in the C_{pm}. The resulting C_{pm} *vs.* T plots reveal a broad feature centered around 2.7 K for the $FeCl_4^-$ salt (Fig. S19), while a sharp λ-type anomaly with a maximum at 5.5 K is observed for the $FeBr_4^-$ salt. Numerical integration of the C_{pm} between 2 and 15 K yields an associated magnetic entropy (S_m), which reaches saturation values of 20.9 and 16.5 J K^{-1} mol^{-1} for the $FeCl_4^-$ and $FeBr_4^-$ salts, respectively (Fig. S20–S21). The estimated entropy gain for the $FeBr_4^-$ salt is very close to R ln6 = 14.9 J K^{-1} mol^{-1}, the value expected for the spin entropy (S = 5/2 Fe^{III} centers), confirming the bulk magnetic order of the Fe^{III} spins. The pronounced entropy contribution observed in the $FeCl_4^-$ salt can be ascribed to factors such as the imprecise estimation of the base line correction (*vide supra*) and/or contributions beyond the purely magnetic component. Another plausible origin is the presence of structural disorder within the system, which not only enhances the overall entropy but also inhibits the stabilization of long-range magnetic order.

Conclusion

We have demonstrated that the electron-rich *peri*-diselenide donor, 2,7-dimethoxynaphthalene *peri*-diselenide (**1**), can be oxidized into stable radical cations to afford 1 : 1 salts with FeX_4^- and GaX_4^- (X = Cl, Br) anions. Theoretical calculations reveal a pronounced localization of the HOMO and spin density on the selenium atoms, where σ-holes simultaneously emerge to engage in chalcogen bond (ChB) with the anions. Structural analysis confirms the presence of short and directional Se···X (X = Cl, Br) ChB interactions around the diselenide bridge with both FeX_4^- and GaX_4^- anions, which effec-

tively bring the anions into close proximity. In addition, strong dimerization of the radical is observed along the stacks of $\mathbf{1}^{\bullet+}$, leaving the FeX_4^- anions as the sole contributors to the magnetic behavior. Magnetic susceptibility and heat capacity measurements suggest that the $FeBr_4^-$ salt undergoes a 3D antiferromagnetic order below T_N = 5.9 K, whereas the $FeCl_4^-$ salt exhibits only short-range correlations above 1.85 K. The stronger magnetic interactions in the $FeBr_4^-$ salt are rationalized by shorter Br···Br contacts. Taken together, these findings demonstrate that the oxidized cation of electron rich diselenides can act as efficient ChB donors, providing a new strategy to control supramolecular organization with magnetic anions and opening perspectives for the design of molecular materials with emergent properties.

Author contributions

H. P. P. synthesized and crystallized the compounds, O. J. performed the crystallographic studies and theoretical calculations, M. R., R. C. and I.-R. J. conducted and analyzed the magnetic and the calorimetric studies, I.-R. J. and M. F. supervised the work. All the authors contributed to the preparation and writing of the manuscript.

Conflicts of interest

There are no conflicts to declare.

Data availability

The data supporting this article have been included as part of the supplementary information (SI). Supplementary information is available: Experimental and synthetic methods, crystallographic and theoretical calculation details, powder X-ray diffraction and magnetostructural correlation data, and additional structural, magnetic, and thermodynamic property data. See DOI: https://doi.org/10.1039/d6dt00277c.

CCDC 2497447 (**1**)(FeCl4), 2497448 (**1**)(GaCl4), 2497449 (**1**)(GaCl4)_B, 2497450 (**1**)(FeBr4) and 2497451 (**1**)(GaBr4) contain the supplementary crystallographic data for this paper.[29a–e]

Acknowledgements

This work received financial support under the EUR LUMOMAT project and the Investments for the Future program ANR-18-EURE-0012 for a PhD grant to H. P. P. This work was granted access to the HPC resources of TGCC/CEA/CINES/IDRIS under the allocation 2024 AD010814136R2 awarded by GENCI. We thank Fatima Awada for preliminary experiments, CDIFX (ISCR) for access to single crystal X-ray diffractometers, and Thierry Guizouarn (ISCR) for transport measurements. R. C., I.-R. J. and M. R. received funding from the University of Bordeaux, Research Program GPR Light (Idex Bordeaux), the Region Nouvelle Aquitaine, Quantum Matter Bordeaux, the ANR (CoordinSCFs project ANR-23-CE07-0029-03 and Magneto-e project, ANR-22-CE07-0050-01), and the Centre National de la Recherche Scientifique (CNRS).

References

1 (*a*) M. Kertesz, Pancake Bonding: An Unusual Pi-Stacking Interaction, *Chem. – Eur. J.*, 2019, **25**, 400–416; (*b*) G. Haberhauer and R. Gleiter, Double Pancake Versus Long Chalcogen–Chalcogen Bonds in Six-Membered C,N, S-Heterocycles, *Chem. – Eur. J.*, 2016, **22**, 8646–8653; (*c*) J. T. Brown, M. Zeller and S. V. Rosokha, Effects of structural variations on π-dimer formation: long-distance multicenter bonding of cation-radicals of tetrathiafulvalene analogues, *Phys. Chem. Chem. Phys.*, 2020, **22**, 25054–25065; (*d*) K. Molčanov, V. Milašinović and B. Kojić-Prodić, Contribution of Different Crystal Packing Forces in π-Stacking: From Noncovalent to Covalent Multicentric Bonding, *Cryst. Growth Des.*, 2019, **19**, 5967–5980.

2 A. Pizzi, G. Terraneo, C. L. Iacono, R. Beccaria, A. Dhaka and G. Resnati, Taxonomy of Chemical Bondings: Opportunities and Challenges, *Angew. Chem., Int. Ed.*, 2025, **64**, e20250652.

3 (*a*) M. Fourmigué and J. Lieffrig, Organizing radical species in the solid state with halogen bonding, *Top. Curr. Chem.*, 2015, **359**, 91–114; (*b*) M. Fourmigué, Organic π-Radicals in the Solid State: From Localized to Delocalized σ-Bonding, in *The Importance of pi-interactions in crystal engineering*, ed. E. R. T. Tiekink and J. Zukerman-Schpector, John Wiley & Sons, Ltd, 2012, ch. 6, pp. 143–162.

4 D. Jérome, Organics Conductors: From Charge Density Wave TTF–TCNQ to Superconducting $(TMTSF)_2PF_6$, *Chem. Rev.*, 2004, **104**, 5565–5591.

5 (*a*) T. Imakubo, H. Sawa and R. Kato, Novel radical cation salts of organic π-donors containing iodine atom(s): the first application of strong intermolecular I···X (X = CN, halogen atom) interaction to molecular conductors, *Synth. Met.*, 1995, **73**, 117–122; (*b*) M. Fourmigué and P. Batail, Activation of Hydrogen- and Halogen-Bonding in Tetrathiafulvalene-Based Crystalline Molecular Conductors, *Chem. Rev.*, 2004, **104**, 5379–5418.

6 (*a*) R. Oliveira, S. Groni, A. Vacher, F. Barrière, D. Lorcy, M. Fourmigué, E. Maisonhaute, B. Schöllhorn and C. Fave, Electrochemical activation of TTF-based XB donors. A powerful, sensitive and selective analytical tool for probing halogen bonding in complex media, *ChemistrySelect*, 2018, **3**, 8874–8880; (*b*) R. Oliveira, S. Groni, C. Fave, M. Branca, F. Mavré, D. Lorcy, M. Fourmigué and B. Schöllhorn, Electrochemical Activation of a Tetrathiafulvalene Halogen Bond Donor in Solution, *Phys. Chem. Chem. Phys.*, 2016, **18**, 15867–15873.

7 (*a*) M. Beau, I.-R. Jeon, O. Jeannin, T. Guizouarn and M. Fourmigué, Activation of chalcogen bonding in tetrathiafulvalene derivatives with Se/S differentiation, *New J. Chem.*, 2025, **49**, 11501–11508; (*b*) M. Beau, S. Lee, O. Jeannin, M. Fourmigué and I.-R. Jeon, Activating both

halogen and chalcogen bonding interactions in cation radical salts of iodinated TTFs, *ChemPlusChem*, 2020, **85**, 2136–2142.

8 (*a*) E. Coronado and P. Day, Magnetic Molecular Conductors, *Chem. Rev.*, 2004, **104**, 5419–5448; (*b*) T. Enoki and A. Miyazaki, Magnetic TTF-Based Charge-Transfer Complexes, *Chem. Rev.*, 2004, **104**, 5449–5477.

9 K. Hervé, O. Cador, S. Golhen, K. Costuas, J.-F. Halet, T. Shirahata, T. Muto, T. Imakubo, A. Miyazaki and L. Ouahab, Iodine Substituted Tetrathiafulvalene Radical Cation Salts with $[M(isoq)_2(NCS)_4]^-$ Anions where M = Cr^{III}, Ga^{III}:Role of I···S and S···S Contacts on Structural and Magnetic Properties, *Chem. Mater.*, 2006, **18**, 790–797.

10 (*a*) N. Hanasaki, H. Tajima, M. Matsuda, T. Naito and T. Inabe, Giant negative magnetoresistance in quasi-one-dimensional conductor $TPP[Fe(Pc)(CN)_2]_2$: Interplay between local moments and one-dimensional conduction electrons, *Phys. Rev. B: Condens. Matter Mater. Phys.*, 2000, **62**, 5839–5842; (*b*) S. Uji, H. Shinagawa, T. Terashima, T. Yakabe, Y. Terai, M. Tokumoto, A. Kobayashi, H. Tanaka and H. Kobayashi, Magnetic-field-induced superconductivity in a two-dimensional organic conductor, *Nature*, 2000, **408**, 447–449; (*c*) G. Kawaguchi, M. Maesato, T. Komatsu, T. Imakubo, A. Kiswandhi, D. Graf and H. Kitagawa, Use of Halogen Bonding in a Molecular Solid Solution to Simultaneously Control Spin and Charge, *Chem. Mater.*, 2016, **28**, 7276–7286.

11 (*a*) A. Miyazaki, H. Yamazaki, M. Aimatsu, T. Enoki, R. Watanabe, E. Ogura, Y. Kuwatani and M. Iyoda, Crystal Structure and Physical Properties of Conducting Molecular Antiferromagnets with a Halogen-Substituted Donor: $(EDO\text{-}TTFBr_2)_2FeX_4$ (X = Cl, Br), *Inorg. Chem.*, 2007, **46**, 3353–3366; (*b*) J. Nishijo, A. Miyazaki, T. Enoki, R. Watanabe, Y. Kuwatani and M. Iyoda, d-Electron-Induced Negative Magnetoresistance of a π–d Interaction System Based on a Brominated-TTF Donor, *Inorg. Chem.*, 2005, **44**(7), 2493–2506.

12 (*a*) M. Maesato, T. Kawashima, Y. Furushima, G. Saito, H. Kitagawa, T. Shirahata, M. Kibune and T. Imakubo, Spin-Flop Switching and Memory in a Molecular Conductor, *J. Am. Chem. Soc.*, 2012, **134**, 17452–17455; (*b*) G. Kawaguchi, M. Maesato, T. Komatsu, H. Kitagawa, T. Imakubo, A. Kiswandhi, D. Graf and J. S. Brooks, Unconventional Magnetic and Resistive Hysteresis in an Iodine-Bonded Molecular Conductor, *Angew. Chem., Int. Ed.*, 2015, **54**, 10169–10172.

13 R. Shukla, A. Dhaka, E. Aubert, V. Vijayakumar, O. Jeannin, M. Fourmigué and E. Espinosa, Understanding Reactivity and Assembly of Dichalcogenides: Structural, Electrostatic Potential and Topological Analyses of 3H-1,2-Benzodithiol-3-one and Se Analogs, *Cryst. Growth Des.*, 2020, **20**, 7704–7725.

14 M. Fourmigué and A. Dhaka, Chalcogen bonding in crystalline diselenides and selenocyanates: from molecules of pharmaceutical interest to conducting materials, *Coord. Chem. Rev.*, 2020, **403**, 213084.

15 L. A. Acampora, B. S. Elman, D. J. Sandman, S. Jansen, M. T. Jones, R. D. Rataiczak and B. M. Foxman, Structural and magnetic studies of electrochemically crystallized halides of 1,4,5,8-tetraselenonaphthalene (TSeN), *Inorg. Chem.*, 1989, **28**, 1579–1582.

16 R. P. Shibaeva and V. F. Kaminskii, Tetraselenatetracene chloride, *Kristallografiya*, 1978, **23**, 1183.

17 (*a*) D. J. Press, T. G. Back and T. C. Sutherland, Charge transfer complexes of electron-rich naphthalene peri-dichalcogenides with TCNQ, *Tetrahedron Lett.*, 2012, **53**, 1603–1605; (*b*) Y. Aso, K. Yui, T. Miyoshi, T. Otsubo, F. Ogura and J. Tanaka, Dichalcogen-Bridged Acenaphthenes as New Electron Donors, *Bull. Chem. Soc. Jpn.*, 1988, **61**, 2013–2018.

18 C. F. L. Male, P. N. Horton, M. B. Pitak, S. J. Coles, S. L. Horswell and R. S. Grainger, [FeFe]-Hydrogenase Synthetic Mimics Based on Peri-Substituted Dichalcogenides, *Organometallics*, 2014, **33**, 4449–4460.

19 The Hamiltonian used in this article including the exchange, Zeeman, and single-ion anisotropy terms is: $H = -2J' \sum_{\langle ij \rangle} S_i \cdot S_j + D \sum_i {S_{i,z}}^2 + g\mu_B H \sum_i S_{i,z}$, where i and j label $S = 5/2$ Fe^{III} spin centers, J' is the average interaction between a spin at site i and its z neighboring spins at sites j, D is the zero-field splitting parameter, g is the Landé factor, and μ_B is the Bohr magneton.

20 H. J. M. De Groot and L. J. De Jongh, Phase diagrams of weakly anisotropic Heisenberg antiferromagnets, nonlinear excitations (solitons) and random-field effects, *Phys. B+C*, 1986, **141**, 1–36.

21 T. Nagamiya, K. Yoshida and R. Kubo, Antiferromagnetism, *Adv. Phys.*, 1955, **4**, 1–112.

22 R. L. Carlin and A. J. Van Duyneveldt, Field-dependent magnetic phenomena, *Acc. Chem. Res.*, 1980, **13**, 231–236.

23 (*a*) M. Wang, X. Xiao, H. Fujiwara, T. Sugimoto, S. Noguchi, T. Ishida, T. Mori and H. A. Katori, Antiferromagnetic or Canted Antiferromagnetic Orderings of Fe(III) d Spins of FeX_4^- Ions in BEDT-TTFVO(S)·FeX_4 (X = Cl, Br) [BEDT-TTFVO(S) = Bis(ethylenedithio)-tetrathiafulvalenoquinone(-thioquinone)-1,3-dithiolemethide], *Inorg. Chem.*, 2007, **46**, 3049–3056; (*b*) Y. Yoshida, M. Maesato, G. Saito and H. Kitagawa, Conducting Coronene Cation Radical Salt Containing Magnetic Metal Ions, *Inorg. Chem.*, 2019, **58**, 14068–14074.

24 D. Wyrzykowski, R. Kruszynski, J. Kłak, J. Mrozinski and Z. Warnke, Structural and magnetic characteristics of tetramethylammonium tetrahalogenoferrates(III), *Inorg. Chim. Acta*, 2008, **361**, 262–268.

25 Z. Warnke, R. Kruszynski, J. Kłak, A. Tomkiewicz and D. Wyrzykowski, Synthesis and magnetic characteristic of new tetrabromo- and tetrachloroferrates(III) with 2-methylquinolinium cation: X-ray crystal structure of bis(2-methylquinolinium) bromide tetrabromoferrate(III), *Inorg. Chim. Acta*, 2006, **359**, 1582–1588.

26 T. Hiraoka, Y. Kamada, T. Matsumoto, H. Fujiwara, T. Sugimoto, S. Noguchi, T. Ishida, H. Nakazumi and

H. A. Katori, Metallic/semiconducting behaviors and an antiferromagnetic ordering of $FeBr_4^-$ d spins in (Benzo-TTFVS)$_2$·M X_4 (M = Fe, Ga; X = Cl, Br), *J. Mater. Chem.*, 2005, **15**, 3479–3487.

27 T. Mori and M. Katsuhara, Estimation of πd-Interactions in Organic Conductors Including Magnetic Anions, *J. Phys. Soc. Jpn.*, 2002, **71**, 826–844.

28 M. Sorai, Y. Nakazawa, M. Nakano and Y. Miyazaki, Calorimetric Investigation of Phase Transitions Occurring in Molecule-Based Magnets, *Chem. Rev.*, 2013, **113**, 41–122.

29 (*a*) CCDC 2497447: Experimental Crystal Structure Determination, 2026, DOI: 10.5517/ccdc.csd.cc2ptst4; (*b*) CCDC 2497448: Experimental Crystal Structure Determination, 2026, DOI: 10.5517/ccdc.csd.cc2ptsv5; (*c*) CCDC 2497449: Experimental Crystal Structure Determination, 2026, DOI: 10.5517/ccdc.csd.cc2ptsw6; (*d*) CCDC 2497450: Experimental Crystal Structure Determination, 2026, DOI: 10.5517/ccdc.csd.cc2ptsx7; (*e*) CCDC 2497451: Experimental Crystal Structure Determination, 2026, DOI: 10.5517/ccdc.csd.cc2ptsy8.